Image Dust Storm Synthetic Method Based on Optical Model

Jiayan Huang[1], Zuoyong Li[2(✉)], and Chuansheng Wang[3]

[1] College of Mathematics and Computer Science, Fuzhou University, Fuzhou 350108, China
jyan_huang@163.com

[2] Fujian Provincial Key Laboratory of Information Processing and Intelligent Control, College of Computer and Control Engineering, Minjiang University, Fuzhou 350121, China
fzulzytdq@126.com

[3] School of Computer Science and Technology, Harbin University of Science and Technology, Harbin 150080, China

Abstract. To address the problem that the dusty image dataset is small and difficult to collect, this paper presents a synthetic method for generating dusty image based on a classical optical model. The proposed method first learns the physical process of generating dusty image according to the classical optical model. Then, the transmission map is estimated and combined with the presupposed dust storm color map as inputs for obtaining a synthetic dusty image. Finally, considering the impact of image scene depth on the synthesis of dusty image, the proposed method selects an appropriate value of input parameter to obtain final synthetic dusty image. Experimental results on an image dataset captured in clear weather show that the synthetic dusty images obtained by the proposed method can be used as a good substitute for real dusty images.

Keywords: Dusty image synthesis · Optical model · Dedusting

1 Introduction

With the development of computer vision and digital image technology, monitoring system can capture clear scenes with more details. For example, car monitoring system can capture the accurate plate numbers and the basic information of other cars in clear weather, which can be considered as valid evidences of violations. However, a dusty weather not only affects the visibility of scene for people, but also the function of computer vision system which is responsible for outdoor monitoring tasks. A majority of existing algorithms focus on image defogging. Despite the fact that dust storm is one of the critical factors which may degrade the performance of outdoor monitoring devices, little attention has been paid to image dedusting, which has resulted in major difficulty in many post-processing

X. Chen et al. (Eds.): ML4CS 2020, LNCS 12488, pp. 215–226, 2020.
https://doi.org/10.1007/978-3-030-62463-7_20

works. Therefore, image dedusting research still has great application prospects in the field of image processing.

The availability of large labeled datasets can advance the research of computer vision. However, it is not yet feasible to annotate such datasets for every new research subject. Thus, focus has been put on learning synthetic data in recent years. Furthermore, synthetic image dataset becomes a good substitute for real dataset in many related experiments. For instance, Jeong et al. [1] adopted a fog synthesis method based on depth information and temporal filtering for road environment. Sakaridis et al. [2] presented a fog synthesis method to obtain a fog simulation image dataset which automatically inherits its true and clear semantic annotations. Besides, for detection of road object in rainy weather, Jeong's method [3] proposes a rainy image synthetic algorithm. And Iizuka et al. [4] tested their proposed image editing system with fog synthesis. Exactly, because of the fact that dusty image data is too small and difficult to collect in reality, the further development of this field has been seriously hindered.

Scattering of particles in atmosphere is the main cause of dust storm. Harald's method [5] finds that lower visibility of foggy images is caused by absorption and scattering of global light by particles in atmosphere. And McCartney et al. [6] explained that the scattering of particles leads to attenuated transmission of light between object and camera, and then adds a layer of atmospherically scattered light. For the problem of lower visibility of foggy image, Nayar et al. [7] explained the imaging process of foggy images with a mathematical model. The atmospheric scattering model provides a powerful basis to develop many algorithms focusing on defogging and even related image processing works, and advances research in this field. Motivated by the success of convolutional neural network (CNN) in feature extraction [8], Ren et al. [9] proposed an image enhancement method based on CNN.

Since similar physical generation process of dust storm and fog, we utilized a standard optical model [10] used in image defogging field to synthesize dusty images. The optical model has been used to model the impact of dust storm on a clear image [9,11,12], and its definition is,

$$I(x) = J(x)t(x) + L(1 - t(x)), \tag{1}$$

where $I(x)$ denotes the observed dusty image at pixel x, $J(x)$ is a clear raw image, L is atmospheric light, and transmission map $t(x)$ is defined as:

$$t(x) = e^{(-\beta l(x))}, \tag{2}$$

where β denotes scattering coefficient of atmosphere, which controls the thickness of dust storm. The larger values of β mean thicker dust storm. As an example, Fig. 1 shows different thickness of dusty scene corresponding to different β. And $l(x)$ is the distance between object and camera. Equation (1) provides a significance basis for simulating dust storm on images with clear-weather.

The main contributions of the paper are: 1) we learn the dusty image model according to classic foggy model, and evaluate the transmission map accurately; 2) we propose a new synthetic method based on classic optical model for dusty

Fig. 1. Synthetic dusty images with different values of β.

images from a clear dataset; 3) we make subjective evaluation and comparison between synthesized dusty images and real dusty scenes, and the final experimental results show that the dusty images synthesized by our approach can be a substitute for real datasets in image dedusting tasks; 4) we extend the dusty image dataset for advancing related post-processing work to some extent.

2 The Proposed Method

Motivated by the classical optical model [10], this paper proposed an image dust storm synthetic method. The required inputs of the proposed synthetic method include an evaluation of the transmission matrix $t(x)$ at each pixel, a hypothetical dust storm color map C, and a clear-weather raw image $J(x)$ for dust storm synthesis. Since the $J(x)$ is simple and easy to be satisfied, we will dedicate to estimate the image transmission t, and selection of dust storm color map C.

Estimation of Transmission: To estimate a transmission map t for the proposed synthetic method, the necessary inputs are:

- an original color image J took in clear-weather as the left image of stereo pair;
- a right image Q for stereo pair;
- the camera focal length f, and two camera baseline b;
- a dense, raw disparity D with the same resolution as the clear image J;
- a set M composed of the pixels without the value of D.

For these required inputs, we can use a stereo camera and standard matching algorithm [13] to acquire them easily.

Before using image depth as input for the calculation of transmission map t, we can improve the quality of depth by using an accurate structure served in color images of stereo pair. Based on this main idea, the main works of our synthetic method can be summarized into five steps:

step1 Calculation of a raw depth map d in meters. According to the principle of stereo image imaging, we use the disparity D in combination with focal length f and the baseline values b of cameras to obtain d by Eq. (3) directly. Those pixels missing disparity D values are also missing depth values in d.

$$d(x) = \frac{b * f}{D(x)}. \tag{3}$$

step2 Estimation of refined depth map $d^{'}$. A segmentation-based depth filling method [2] based on the stereoscopic inpainting method [14] be used in this step. Specifically, we use a superpixel segmentation of the clear image J to guide the denoising and completion of d at the superpixel level, and make an assumption that each individual superpixel corresponding to a plane in the 3D scene.

Firstly, we check photo-consistency between J and Q, all pixels in J whose color deviation (measured in RGB color space) is greater $\epsilon = 12/255$ from the corresponding pixel in Q are considered invalid in image depth, and are added to set M.

Secondly, we implement SLIC [15] to segment clear image J into superpixels. $\widehat{K}$ denotes the expected number of superpixels and m is the related range domain scale parameter, respectively (set $\widehat{K} = 2048$ and $m = 10$). The final output number of superpixels of SLIC is represented as K. According to the number of invalid or missing depth pixels in a superpixel, all superpixels are classify into reliable and unreliable. A surperpixel T is regarded as a reliable superpixel if and only if the following condition [14] is satisfied:

$$T_{rel} = \begin{cases} 1, & card(T \backslash M) \geq max\{P, \lambda card(T)\} \\ 0, & otherwise \end{cases} \tag{4}$$

where $card(\cdot)$ denotes the number of pixels in a set, $T \backslash M$ is the set difference between T and M, setting $P = 20$ and $\lambda = 0.6$.

In order to fit a depth plane for each superpixel, we run RANSAC (Random Sample Consensus) on its pixels with valid depth value, and account for differences in the range of depth values between distinct superpixels by an adaptive inlier threshold defined as:

$$\theta = 0.01 \underset{x \in T \backslash M}{median}\{d(x)\}, \tag{5}$$

where $d(x)$ denotes the estimated depth of superpixel x. By using adaptive RANSAC, the maximum number of iterations is set to 2000, and the bound of probability $p = 0.99$ for obtaining a pure sample.

We then use a greedy algorithm [9] to match unreliable superpixels to reliable ones pairwise, and assign the fitted depth plane of reliable superpixel to its matched unreliable superpixel. Different from the method [14], we apply a novel objective function [2] for matching of superpixel pair (s, t), which is defined as:

$$E(s,t) = ||C_s + C_t||^2 + \alpha||x_s + x_t||^2. \tag{6}$$

The first term on right-hand side of Eq. (6) is used to describe the similarity between two superpixels in color space, C_s denotes the average CIELAB color of the superpixel s. More specifically, the method [2] penalized the squared Euclidean distance of the average colors of two superpixels in CIELAB color space for increasing perceptual uniformity while another method [14] designs its cost of range domain by using cosine similarity of average colors of superpixels:

$$E_{cls}(s,t) = 1 - \frac{C_s}{||C_s||} \cdot \frac{C_t}{||C_t||}. \tag{7}$$

where $E_{cls}(s,t)$ is the color similarity between the two superpixels, C_s and C_t are the average color vectors of superpixels s and t, respectively. In some cases, Eq. (7) exists a problem that it may assign zero matching penalty to dissimilar colors. For example, in the RGB color space, the pair of colors (δ, δ, δ) and $(1-\delta, 1-\delta, 1-\delta)$, where δ is a small positive constant is assigned zero match cost, even though the former color is very dark grey and the latter is very light grey.

The second term on right-hand side of Eq. (6) calculates the squared Euclidean distance between two centroid x_s and x_t of superpixel pair (s, t) in spatial space, which be used to denote the similarity of two superpixels. Due to the Eq. (7) gives zero matching penalty to adjacent superpixel and unit cost to non-adjacent superpixel, a superpixel s will mismatch a far superpixel t as long as the range domain of superpixel pair is minimum and has a different appearance with all adjacent superpixels of s. On the contrary, the method [2] handled well for the problem that existed in [14], i.e. other superpixels with less similar appearance yet smaller distance to s will be the first choice if t has a large spatial cost to matching s.

The parameter $\alpha > 0$ in Eq. (6) is used to balance the importance between spatial space and color space. Let $\alpha = m^2/S^2$, where $S = \sqrt{N/K}$, N is the total number of pixels in the image, m and K are the same as for SLIC [15]. The matching target of Eq. (6) is similar to the distance defined in SLIC. In this paper, we use this distance to measure the similarity of superpixel pair.

After all superpixels have been assigned a depth plane, we use these planes to complete the missing depth values of pixels belonging to set M. Besides, the depth values of those pixels, which do not belong to M but constitute large-margin outliers with their corresponding plane (deviation larger than $\widehat{\theta} = 50$ m) are replaced with the values imputed by the plane, and finally results in a denoising and complete depth map $d^{'}$.

step3 Computation of scene distance $l(x)$ from camera. Each pixel value in the depth map $d^{'}$ represents the distance between a point in the scene and the

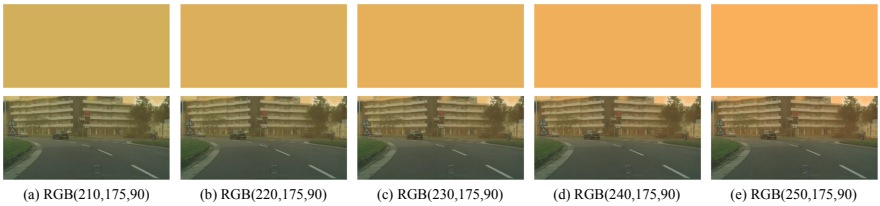

Fig. 2. Different hypothetical dust storm color maps and their corresponding synthetic dusty images. (Color figure online)

camera. Therefore, we use the coordinates of principal point that takes the center point of the image as the coordinate origin, and the focal length of camera to calculate the distance $l(x)$ of scene from camera at each pixel x based on $d^{'}(x)$.

step4 Calculation of initial transmission map $\widehat{t}$. We can substitute $l(x)$ into Eq. (2) to obtain an initial transmission map $\widehat{t}$.

step5 Guided filter of $\widehat{t}$ using J as guidance to compute the final transmission $t(x)$. In order to smooth transmission $t(x)$ while preserving boundaries of clear image J, a guided filtering [16] is used for the post-process of the initial transmission $\widehat{t}$. We set the radius of guided filter window to $r = 20$, and regularization parameter to $\mu = 10^{-3}$ (the same values as the haze removal experiments of [16]). The results in a final transmission map $t(x)$.

Selection of Dust Storm Color Map: As Fig. 2 shows, we further compare various possible dust storm colors and select the final hypothetical dust storm color map C for our dusty image synthetic method. According to our observation on a large number of real dusty images, the dust storm color is generally pale orange, and the red in RGB color space has the main impact on pale orange. Therefore, we respectively fixed the green and blue color values at 175 and 90, and changed the red color value within the possible color range of dust storm to obtain different dust storm color maps. The second row of the Fig. 2 gives the corresponding synthetic results of different hypothetical dust storm color maps. Considering the color of most real dusty scenes, we selects the RGB value of (230, 175, 90) as the input dust storm color map.

Considering the impact of the proposed method on synthetic image depth, a parameter λ is introduced based on Eq. (1). Therefore, the equation transformed into the following expression:

$$I(x) = J(x)(1 - \lambda(1 - t(x))) + \lambda C(1 - t(x)), \tag{8}$$

where $I(x)$ is the target synthetic dusty image, $J(x)$ is the original clear image, and C denotes the hypothetical dust storm color of the proposed method, λ is a parameter. As shown in Fig. 3, it is a whole flow chart of the proposed dusty image synthetic method.

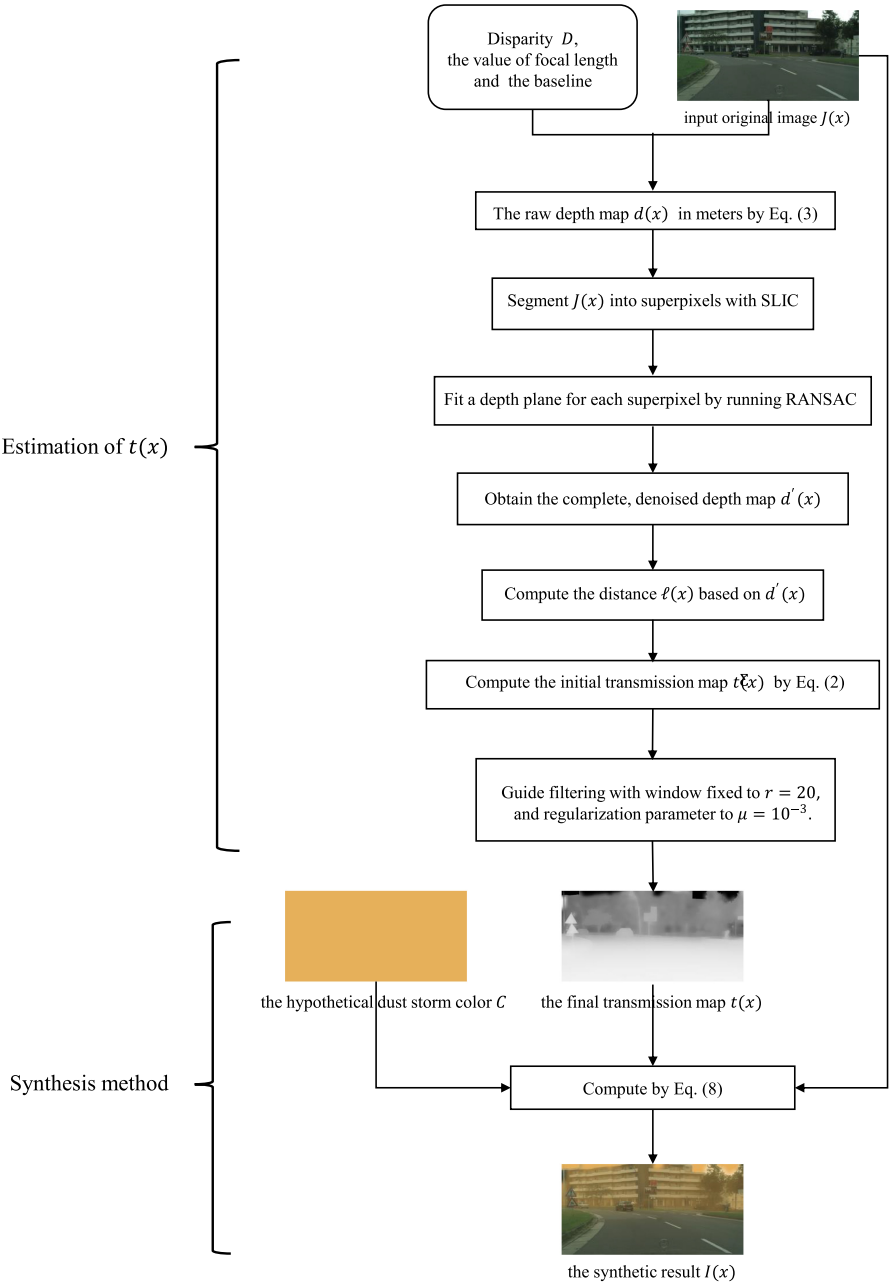

Fig. 3. The flow chart of the proposed dusty image synthetic method.

3 Experimental Results

3.1 Evaluation of Dusty Image Synthesis

To validate effectiveness of the proposed image dust storm synthetic method, five typical images are chosen as testing samples. Five images have the following characteristics: (1) they are from different image scenes. In detail, the first image is captured in a road scene, the second image is captured in wall scene, the third image is capture in city scene, the fourth image is captured in street scene, and the fifth image contain close shot details. (2) They are color image. Therefore, they can be used to observe dusty image synthesis on image details. (3) The third and fourth images have not sky region, and the former two images have large sky regions, which can be used to observe color distortion in sky regions. (4) The second image contains sharp shadows, and the other images have not sharp shadows, which can obtain more realistic image dusty synthetic results.

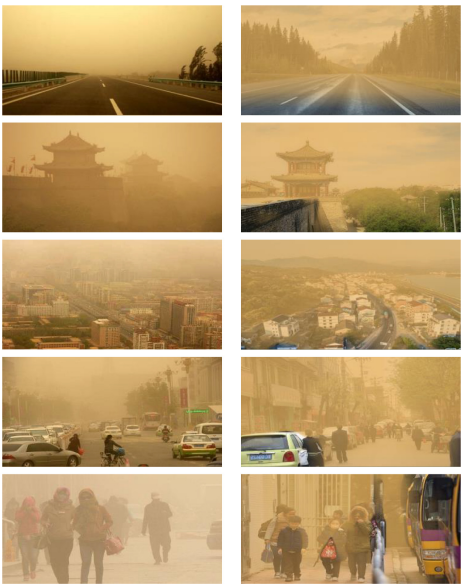

Fig. 4. Comparison of real dusty images and the synthetic dusty images obtained by the proposed method.

As far as we know, there are few or even no existing image dust storm synthesis algorithms to validate superiority of the proposed dusty image synthetic method. Therefore, image dusty storm synthetic results were qualitatively evaluated. As Fig. 4 shows, we compare dusty images obtained by the proposed method with real dusty images downloaded randomly from the internet. From Fig. 4, we can observe that image dust storm synthetic results obtained by the

proposed method eliminate color distortion in sky regions, and make image detail visible. As compared with the real-world dusty scenes, the synthetic dusty images obtained by the proposed method can be a substitute for real dusty images in many dedusting related post-processing tasks.

3.2 Parameter Discussion

We further discuss the influence of parameter λ on the results of dust storm synthesis in this section, and find an ideal value of λ for the proposed dusty image synthetic method to improve the visual results of synthetic dusty images.

During the specific synthetic experiment, we first use different values of the parameter λ (0.4, 0.6, 0.8 and 1.0) for obtaining dusty images with different qualities. Figure 5 shows dust storm synthetic results from clear images, the columns from left to right are the original images and the synthetic dusty images obtained by the proposed method with $\lambda = 0.4$, $\lambda = 0.6$, $\lambda = 0.8$, and $\lambda = 1.0$.

According to Eq. (8) and Fig. 5, we can intuitively find that the higher the value of λ is, the larger the weight of the hand-right term of Eq. (8), thus resulting in thicker dust storm on the synthetic image. On the contrary, higher weight of the hand-left term of Eq. (8) indicates lower dusty thickness in synthetic dusty image. Therefore, we draw a hypothetical conclusion that the damage to the original image depth by the synthetic dusty image increases with the increase of λ value.

Fig. 5. The visual synthetic dusty images with different λ values obtained by the proposed method.

And then, in order to obtain more reliable value of λ for higher quality of simulation results, we use an existing depth estimation method [17] to obtain the depth maps of original image and its different synthetic results of different values of λ. An example of the corresponding depth maps is illustrated in Fig. 6.

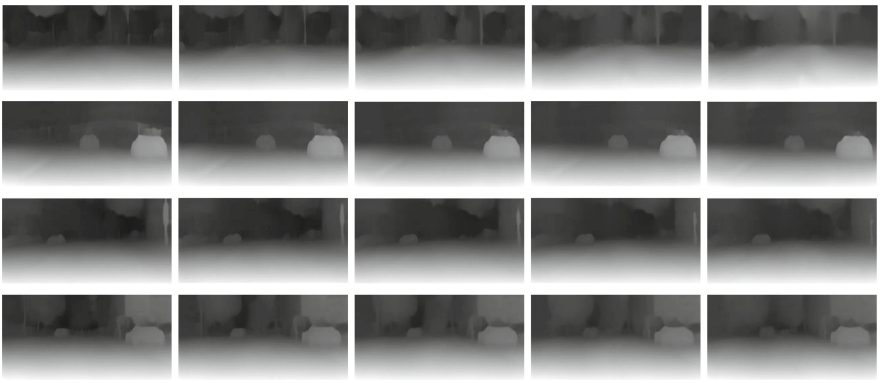

Fig. 6. The scene depth estimation maps of original images and corresponding synthetic dusty images with different λ values.

Image depths were quantitatively evaluated. Four commonly used indexes (including the Root Mean Squared Error (RMSE), Log Root Mean Squared Error (RMSE_log), Square Relative Error (Sq_Rel), and Absolute Relative Error (Abs_Rel)) are adopted as the evaluation criteria for comparison of depth map, where the smaller the values of all these indexes are, the less is the depth map of the original image damaged by the proposed dusty image synthetic method.

Table 1. Average absolute difference of scene depth between original image and synthetic dusty images with different λ values.

λ	RMSE	RMSE_log	Abs_Rel	Sq_Rel
0.4	4.731	0.147	0.023	0.077
0.6	6.509	0.188	0.056	0.121
0.8	9.591	0.228	0.120	0.168
1.0	11.881	0.255	0.224	0.236

Finally, by using the four evaluation indexes mentioned above, we quantitatively compare original clear image with four different depth maps of dusty images obtained by the proposed method, and the results are shown in Table 1. It can be found from the data in Table 1, as we set the parameter value higher, the four indexes become larger as well, which means that the synthetic dusty image obtained with the high-value parameter will cause more serious damage to the original image depth map. To sum up, we validate the previous assumption that the dusty images with higher quality and similarity to the dusty scenes in real world can be obtained when we set the input parameter $\lambda = 0.4$.

4 Conclusion

In this paper, we proposed a novel method for generating synthetic dusty images to alleviate the difficulty of collecting dusty images in image dedusting task needing a lot of dusty images. Specifically, the proposed method constructed a mathematical model of dusty image generation according to the classical optical model, and estimated the transmission map of original clear image for the generation of final synthetic dusty images. We qualitatively compared the synthetic dusty images obtained by the proposed method and real dusty images. Experimental results on a series of original images captured in clear weather demonstrate that the synthetic dusty images obtained by the proposed method can be used as a good substitute for real dusty images. In the future, we will try to improve the proposed synthetic method, and use deep learning based image dedusting methods to verify the effectiveness of synthetic data for improving image dedusting effect.

Acknowledgment. This work is partially supported by National Natural Science Foundation of China (61972187, 61772254), Fujian Provincial Leading Project (2017H0030, 2019H0025), Government Guiding Regional Science and Technology Development (2019L3009), and Natural Science Foundation of Fujian Province (2017J01-768 and 2019J01756).

References

1. Jeong, K.M., Song, B.C.: Fog detection and fog synthesis for effective quantitative evaluation of fog-detection-and-removal algorithms. IEIE Trans. Smart Process. Comput. **7**(5), 350–360 (2018)
2. Sakaridis, C., Dai, D., Van Gool, L.: Semantic foggy scene understanding with synthetic data. Int. J. Comput. Vis. **126**(9), 973–992 (2018)
3. Jeong, K.M., Song, B.C.: Image synthesis algorithm for road object detection in rainy weather. IEIE Trans. Smart Process. Comput. **7**(5), 342–349 (2018)
4. Iizuka, S., Endo, Y., Hirose, M., Kanamori, Y., Mitani, J., Fukui, Y.: Object repositioning based on the perspective in a single image. Comput. Graph. Forum **33**, 157–166 (2014)
5. Harald, K.: Theorieder horizontalen sichtweite: Kontrast und sichtweite, vol. 12. Keim & Nemnich, Munich (1924)
6. McCartney, E.J.: Optics of the Atmosphere: Scattering by Molecules and Particles, p. 421. Wiley, New York (1976)
7. Nayar, S.K., Narasimhan, S.G.: Vision in bad weather. In: Proceedings of the Seventh IEEE International Conference on Computer Vision, vol. 2, pp. 820–827. IEEE (1999)
8. Ning, X., Li, W., Tang, B., He, H.: BULDP: biomimetic uncorrelated locality discriminant projection for feature extraction in face recognition. IEEE Trans. Image Process. **27**(5), 2575–2586 (2018)
9. Ren, W., Liu, S., Zhang, H., Pan, J., Cao, X., Yang, M.-H.: Single image dehazing via multi-scale convolutional neural networks. In: Leibe, B., Matas, J., Sebe, N., Welling, M. (eds.) ECCV 2016. LNCS, vol. 9906, pp. 154–169. Springer, Cham (2016). https://doi.org/10.1007/978-3-319-46475-6_10

10. Koschmieder, H.: Theorie der horizontalen sichtweite, beitrage zur physik der freien atmosphare. Meteorologische Zeitschrift **12**, 3353 (1924)
11. He, K., Sun, J., Tang, X.: Single image haze removal using dark channel prior. IEEE Trans. Pattern Anal. Mach. Intell. **33**(12), 2341–2353 (2010)
12. Fattal, R.: Single image dehazing. ACM Trans. Graph. (TOG) **27**(3), 1–9 (2008)
13. Hirschmuller, H.: Stereo processing by semiglobal matching and mutual information. IEEE Trans. Pattern Anal. Mach. Intell. **30**(2), 328–341 (2007)
14. Wang, L., Jin, H., Yang, R., Gong, M.: Stereoscopic inpainting: joint color and depth completion from stereo images. In: Proceedings of the IEEE Conference on Computer Vision and Pattern Recognition, pp. 1–8. IEEE (2008)
15. Achanta, R., Shaji, A., Smith, K., Lucchi, A., Fua, P., Süsstrunk, S.: SLIC superpixels compared to state-of-the-art superpixel methods. IEEE Trans. Pattern Anal. Mach. Intell. **34**(11), 2274–2282 (2012)
16. He, K., Sun, J., Tang, X.: Guided image filtering. IEEE Trans. Pattern Anal. Mach. Intell. **35**(6), 1397–1409 (2012)
17. Godard, C., Mac Aodha, O., Firman, M., Brostow, G.J.: Digging into self-supervised monocular depth estimation. In: Proceedings of the IEEE International Conference on Computer Vision, pp. 3828–3838 (2019)